Rapid and Sustained Nuclear-Cytoplasmic ERK Oscillation Induced by Epidermal Growth Factor

Harish Shankaran[§], Danielle L. Ippolito[§], William B. Chrisler[§], Haluk Resat[§], Nikki Bollinger[§], Lee K. Opresko[§] and H. Steven Wiley[§¶]

[§]Systems Biology Program and [¶]Environmental Molecular Sciences Laboratory, Pacific Northwest National Laboratory, Richland, WA 99352

SUPPLEMENTARY INFORMATION

Contents:

SUPPLEMENTARY FIGURES

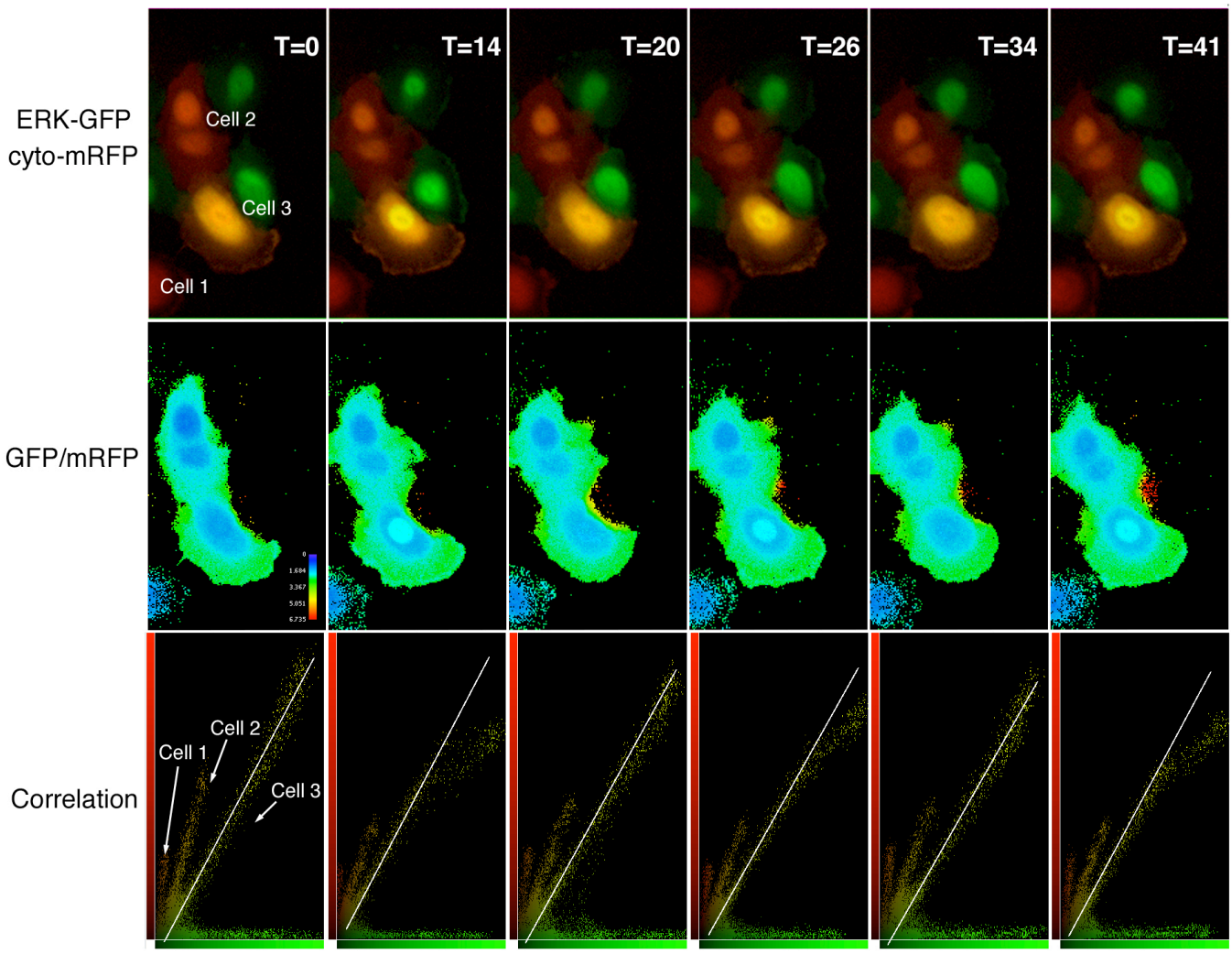

Supplementary Figure S1. Ratio of ERK-GFP and cytoplasmic mRFP after EGF addition. Cells expressing both markers were treated with 1ng/ml of EGF for the time indicated at the top. Both the green and red fluorescence channels were acquired and processed with Volocity software. Top panels are the original fused images. Middle panels are the ratio of GFP:mRFP intensity. Bottom panel is a pixel-by-pixel correlation profile of the entire image. The line in the bottom panel is constant to serve as a reference. In cell #3, the ratio at 0-time ranged from 1.45 in the nucleus to approximately 1.7 in the perinuclear region and cell periphery. Following EGF addition, the nuclear ERK-GFP/mRFP ratio rose to over 2 and the perinuclear ratio dropped to 1.55.

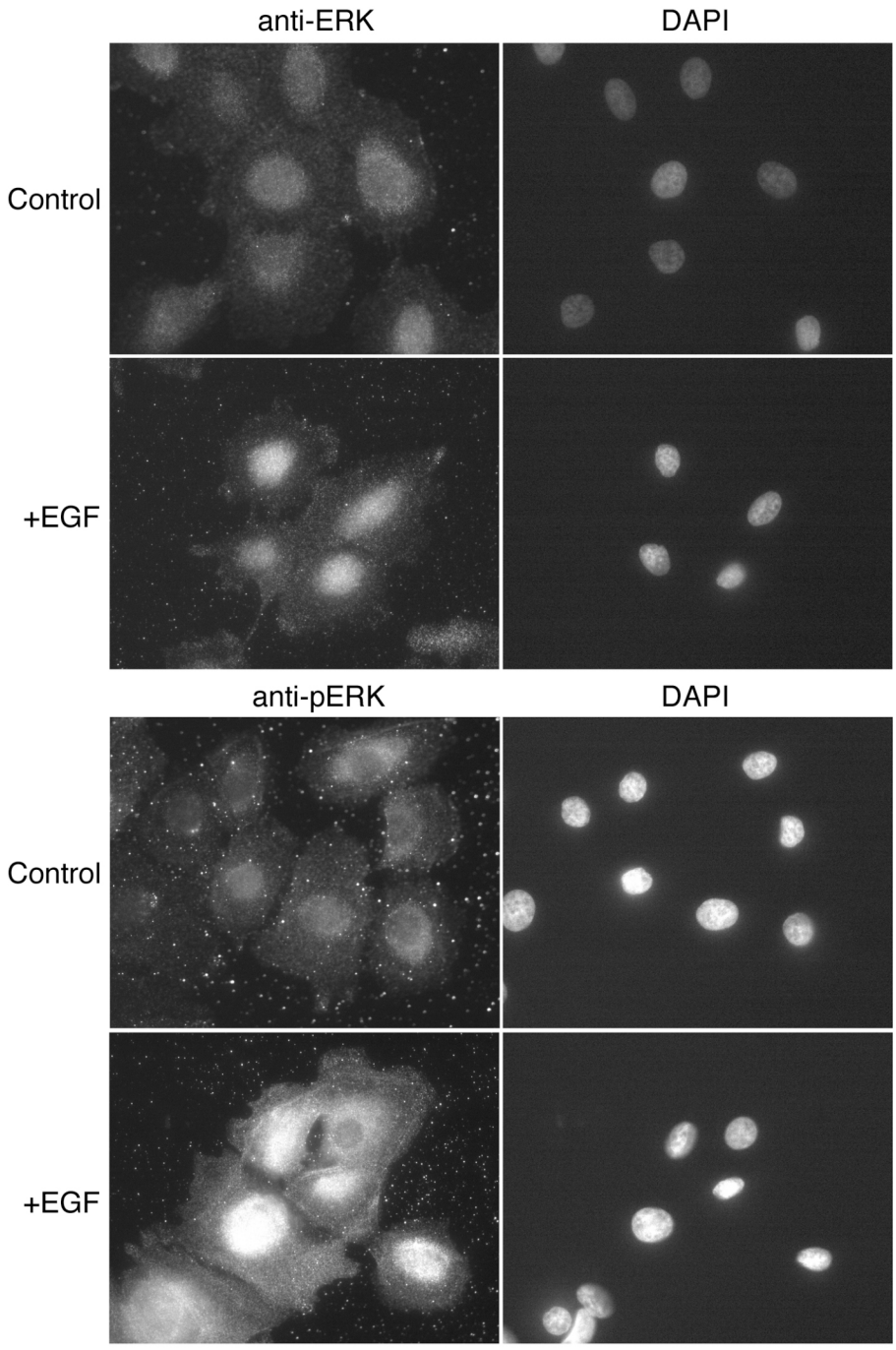

Supplementary Figure S2. EGF stimulation results in an increased level of both total and phosphorylated ERK in the nucleus of HMEC. Parental cells were treated with or without 1 ng/ml of EGF for 20 min at 37°C and then fixed and permeabilized as described in *Supplementary Methods* to visualize the intracellular localization of total ERK and phopho-ERK by confocal microscopy. Cells were also counterstained with DAPI to visualize the nuclei.

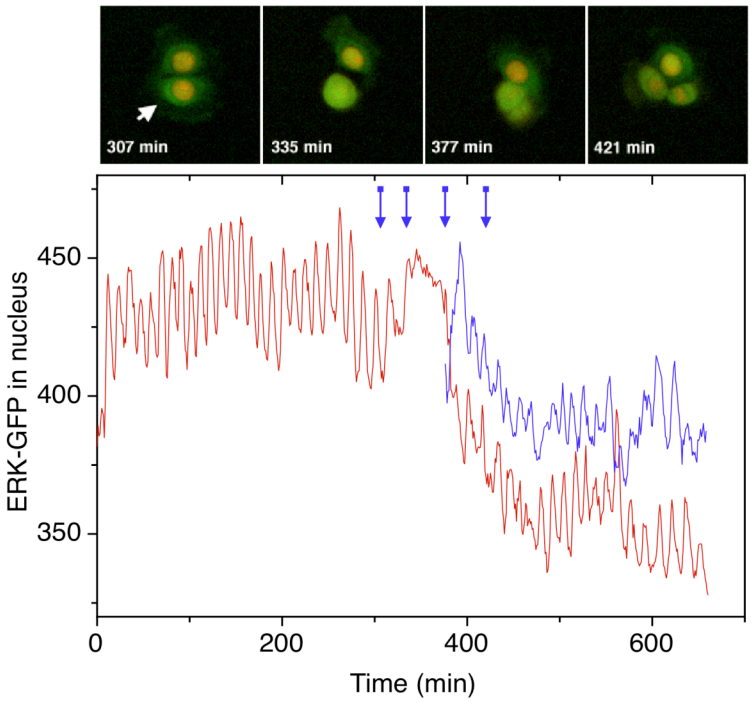

Supplementary Figure S3. Oscillations persist through mitosis. The nuclear level of ERK-GFP in a cell that divided during the observation period is shown with the levels in the resulting daughter cells. The four images in the upper panel correspond to the four arrows in the lower panel. The lack of oscillations from 335-377 minutes corresponds to the dissolution of the nuclear envelope during mitosis.

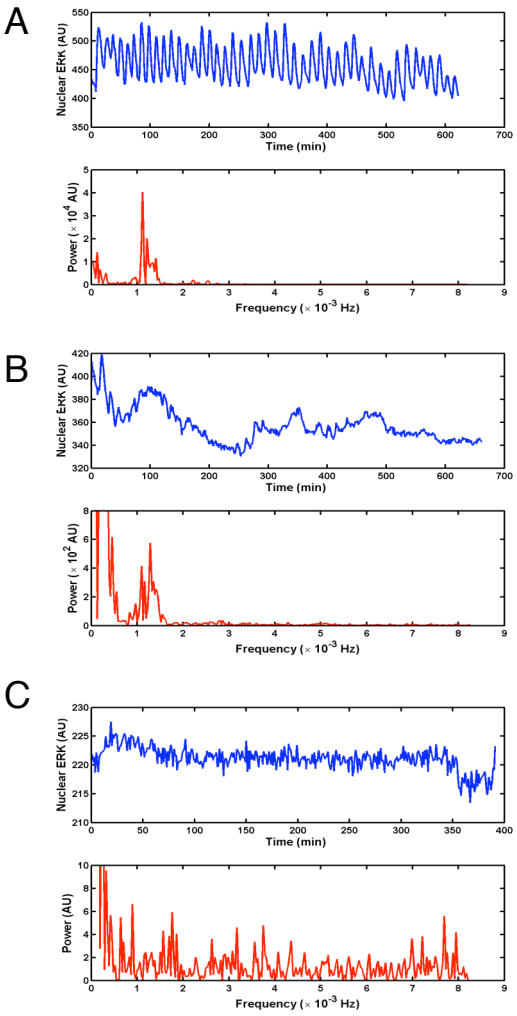

Supplementary Figure S4. Fourier-based classification scheme for ERK oscillations. **(A)** Example of a "clean" oscillation. Upper panel is the original data set and the bottom panel is the Fourier transform of the data. Note the narrow frequency spectrum. **(B)** Example of a "noisy" oscillation. Upper panel is the original data set and the bottom panel is the Fourier transform of the data. Note that the peak between 1-2 x 10^{-3} H is less prominent than lower frequencies. **(C)** Example of no oscillation. Upper panel is the original dataset and the bottom panel is the Fourier transform of the data. Note the lack of any dominant frequency component.

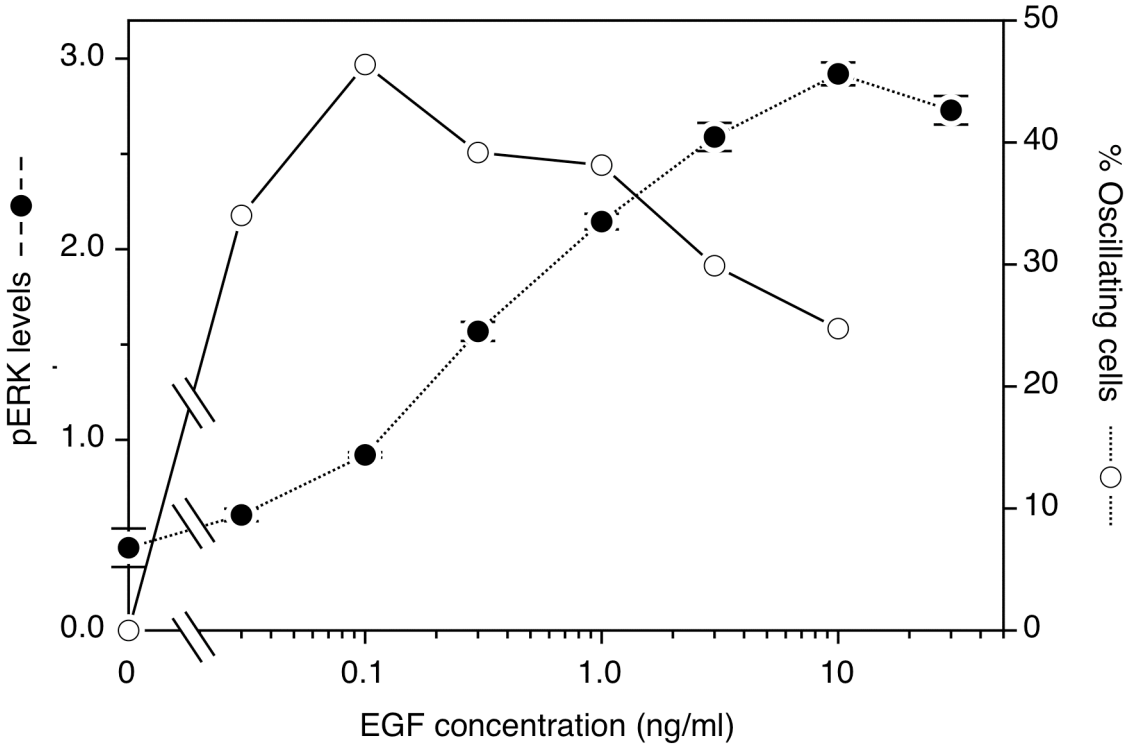

Supplementary Figure S5. Effect of EGF concentration on ERK phosphorylation versus ERK-GFP oscillations. For the measurement of ERK phosphorylation, cells were grown to approximately 45% confluency and treated for 30 minutes with the indicated concentration of EGF prior to cell lysis. The levels of phospho-ERK (solid circles) in triplicate samples were then measured by ELISA as described in Materials and Methods. Cells expressing ERK-GFP were grown under the same conditions and confluency and treated with step changes in EGF concentrations at 90 min intervals. The percentage of clean oscillations observed for a total of 97 cells in 4 separate fields were then calculated as described in Materials and Methods.

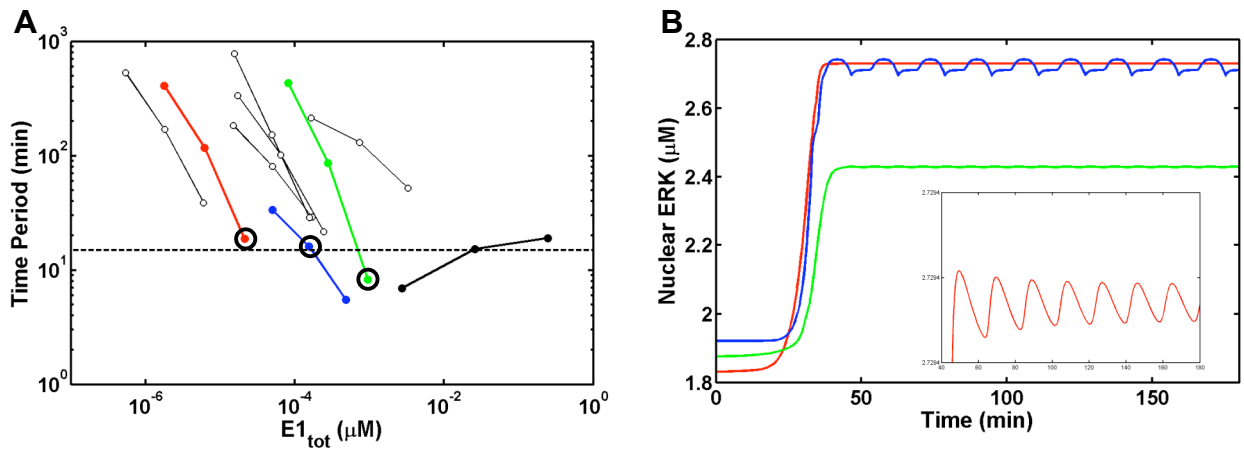

Figure. S6. Oscillations in the absence of negative feedback. We removed the negative feedback in the mathematical model and generated 10,000 parameter sets by allowing the biochemical parameters to vary in a 2-orders of magnitude range around the base value. During this sampling, ERK and MEK concentrations were kept fixed, and Raf levels were allowed to vary from 1/3 to 3-times the base value. **(A)** The time period is plotted as a function of the input strength for the 8 parameter sets that show oscillations over at least a 10-fold increase in input strength. Results are also shown for the base parameter set (dark black line) with negative feedback for comparison. Three of the non-negative feedback parameter sets (red, blue and green) display a time period close to 15 min within their respective oscillatory regimes. **(B)** Nuclear ERK profiles are presented for the three candidate parameter sets at the input strengths indicated by the black circles in panel A. Inset in panel B is an expanded view of the red profile highlighting the presence of an oscillation (albeit with an extremely small amplitude).

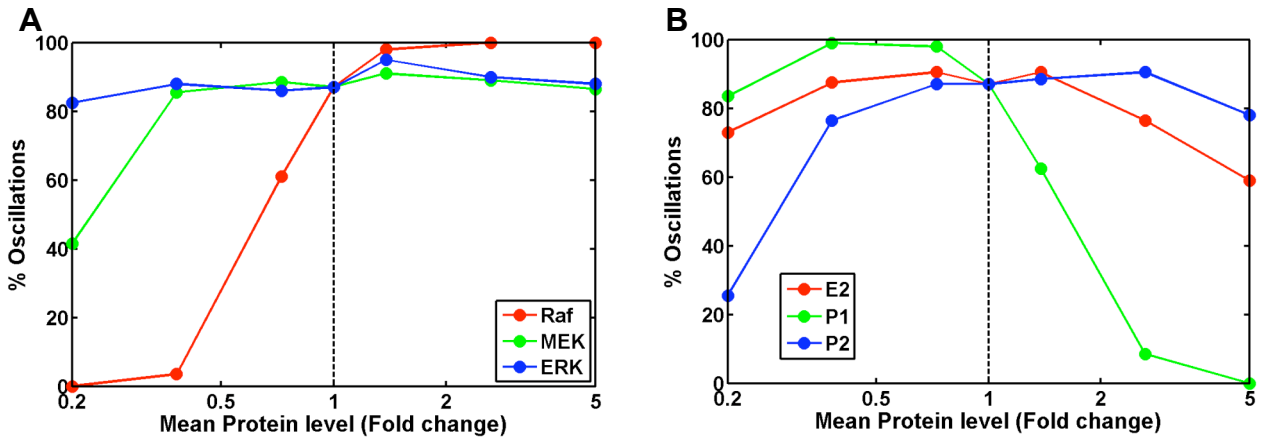

Figure. S7. Sensitivity of ERK oscillations to changes in kinase and phosphatase abundances. We constructed altered parameter sets by varying each of the three kinase and phosphatase abundances one at a time from 1/5 to 5-times their value in the base parameter set. We then set the input strength $E1_{tot}$ at 0.02 μM, and generated 100 "cells" with inputs log-normally distributed around $E1_{tot}$ and parameters log-normally distributed around the appropriately altered base set. We determined the total percentage of oscillations using these 100 theoretical cells for each condition. The total oscillation percentage is plotted as a function of the fold change in protein level for the 3 kinases (**A)** and 3 phosphatases (**B)** in the ERK cascade.

SUPPLEMENTARY METHODS

Immunofluorescence of total and phosphorylated ERK

HMEC 184 A1 cells (passage 50) were plated onto sterile glass coverslips and allowed to attach for 4 hours in DFCI-1 (see Materials and Methods in the main text). After 4 hours, the media was replaced with DFCI-1 without EGF and grown overnight. The cells were then treated with EGF at a final concentration of 1 ng/ml. The cells were then washed with phosphate-buffered saline (PBS) and fixed with 3.6% paraformaldehyde containing 0.024% saponin and 1 mM sodium orthovanadate. The slides were blocked for 1 hour with 1% BSA in PBS. The cells are then incubated with antibodies against total ERK (Cell Signaling Antibody #9102) diluted 1:50 or phosphorylated ERK (Cell Signaling Antibody #9106) diluted 1:200 overnight at 4°C. The cells were then washed and incubated with fluorescent secondary antibodies. Alexa Fluor 488 goat anti-rabbit IgG (H+L) for total ERK, and Alexa Fluor 488 goat anti-mouse IgG (H+L) for phosphorylated ERK. The cells were then imaged using a Leica DMIRE2 confocal microscope.

Waveform classification and frequency determination using Fourier analysis

Nuclear ERK time-series data were analyzed to identify oscillating cells in the population using the fast Fourier transform (FT) function of the MATLAB software. For each cell, the ERK time series and the corresponding FT spectrum were examined and the cell was manually assigned to one of three categories: 1) clean oscillation 2) noisy oscillation and 3) non-oscillatory. A cell that displayed sustained oscillations with clearly discernible peaks and valleys in the time-series and in addition had a sharp FT peak at a time period of <30 minutes was deemed a clean oscillator. For these clean oscillators the start and end times of the oscillations in the time series were manually located and stored. Some cells displayed a clear FT peak at a time-period of < 30 minutes, but the oscillations in the time domain were of low amplitude and/or were noisy. These cells were classified as noisy oscillators. Cells that did not fit either of the aforementioned categories were classified as being non-oscillatory. The FT peak was used to estimate the time period of the oscillation for both clean and noisy oscillators. It should be noted that the time period computed using the FT peak reflects the characteristics of the time series on average, and does not report on the shapes and time periods of the individual oscillation pulses in the data.

Time period, amplitude and pulse shape determination for clean oscillators

Previously identified clean oscillations of sufficient dynamic range were analyzed in defined oscillation time windows using custom MATLAB routines to characterize the oscillation waveform. The locations of the peaks and valleys in the time series were first automatically determined by identifying points of inflection in a piecewise quadratic fit of the data. Parabolic curves were fitted to the time series 5 points at a time. Strong extrema in the time series appeared as inflections in successive piecewise fits and were retained for further analysis. The locations of the extrema were further filtered to ensure that the time series contained alternating sets of peaks and valleys. If there were two successive peaks (or valleys) in the time series then the highest (lowest) of these peaks (valleys) was retained. The locations of the i^{th} peak and the i^{th} valley on the time axis were denoted as $t_{p(i)}$ and $t_{v(i)}$, respectively. These locations were used to compute the time periods of the individual pulses. Oscillation series were set to commence with a valley. The i^{th} pulse in such an oscillation series comprises the valleys $t_{v(i)}$ and $t_{v(i+1)}$ and has an intermediate peak at $t_{p(i)}$. We computed the time period of the i^{th} pulse as $T_i = t_{v(i+1)} - t_{v(i)}$.

In addition, we computed the rise and decay times for the i^{th} pulse as $R_i = t_{p(i)} - t_{v(i)}$ and $D_i = t_{v(i+1)} - t_{p(i)}$. Once the time period and rise and decay times were obtained for all the pulses in the time series, the results were combined to determine means ($\langle R_i \rangle$, $\langle D_i \rangle$, $\langle T_i \rangle$) and standard deviations of these quantities for each cell.

We determined the response value at the midpoint times in the rise and decay phases of each pulse to obtain estimates of how the mean ERK-GFP level, $Y_{mean}(t)$ changed as a function of time. We fitted a piecewise cubic polynomial through the Y_{mean} vs t curve to enable interpolation. The amplitude of each pulse was determined as the difference between the actual nuclear ERK-GFP level and the estimated Y_{mean} value at the pulse peak, i.e. $A_i = y(t_{p(i)}) - Y_{mean}(t_{p(i)})$. We computed a normalized amplitude A_i^* for each pulse as $A_i^* = A_i / Y_{mean}(t_{p(i)})$. We averaged these normalized pulse amplitudes to obtain a mean amplitude $\langle A_i^* \rangle$ value for each cell. A similar protocol was used to quantify the time periods, rise times, decay times and amplitudes of oscillations generated by our mathematical model.

Model development, bifurcation analysis and simulations

Our model for the MAPK pathway combines elements from the models constructed by Huang and Ferrell (Huang & Ferrell, 1996; Qiao *et al*, 2007) and Fujioka *et al.* (Fujioka *et al*, 2006). The enzymatic phosphorylation and dephosphorylation reactions in our model are similar to those described by Qiao et al. (Qiao *et al*, 2007), and are listed below:

$$\text{MKKK} + \text{E1} \underset{d_1}{\overset{a_1}{\rightleftharpoons}} \text{MKKK}\cdot\text{E1} \xrightarrow{k_1} \text{MKKK}^* + \text{E1} \quad (1)$$

$$\text{MKKK}^* + \text{E2} \underset{d_2}{\overset{a_2}{\rightleftharpoons}} \text{MKKK}^*\cdot\text{E2} \xrightarrow{k_2} \text{MKKK} + \text{E2} \quad (2)$$

$$\text{MKK} + \text{MKKK}^* \underset{d_3}{\overset{a_3}{\rightleftharpoons}} \text{MKK}\cdot\text{MKKK}^* \xrightarrow{k_3} \text{MKK-P} + \text{MKKK}^* \quad (3)$$

$$\text{MKK-P} + \text{P1} \underset{d_4}{\overset{a_4}{\rightleftharpoons}} \text{MKK-P}\cdot\text{P1} \xrightarrow{k_4} \text{MKK} + \text{P1} \quad (4)$$

$$\text{MKK-P} + \text{MKKK}^* \underset{d_5}{\overset{a_5}{\rightleftharpoons}} \text{MKK-P}\cdot\text{MKKK}^* \xrightarrow{k_5} \text{MKK-PP} + \text{MKKK}^* \quad (5)$$

$$\text{MKK-PP} + \text{P1} \underset{d_6}{\overset{a_6}{\rightleftharpoons}} \text{MKK-PP}\cdot\text{P1} \xrightarrow{k_6} \text{MKK-P} + \text{P1} \quad (6)$$

$$\text{ERK} + \text{MKK-PP} \underset{d_7}{\overset{A_7,\, K_{S7}}{\rightleftharpoons}} \text{ERK}\cdot\text{MKK-PP} \xrightarrow{k_7} \text{ERK-P} + \text{MKK-PP} \quad (7)$$

$$\text{ERK-P} + \text{P2} \underset{d_8}{\overset{a_8}{\rightleftharpoons}} \text{ERK-P}\cdot\text{P2} \xrightarrow{k_8} \text{ERK} + \text{P2} \quad (8)$$

$$\text{ERK-P} + \text{MKK-PP} \underset{d_7}{\overset{A_9,\, K_{S9}}{\rightleftharpoons}} \text{ERK-P}\cdot\text{MKK-PP} \xrightarrow{k_7} \text{ERK-PP} + \text{MKK-PP} \quad (9)$$

$$\text{ERK-PP} + \text{P2} \underset{d_{10}}{\overset{a_{10}}{\rightleftharpoons}} \text{ERK-PP}\cdot\text{P2} \xrightarrow{k_{10}} \text{ERK-P} + \text{P2} \quad (10)$$

$$\text{ERK} + \text{MKK} \underset{d_{11}}{\overset{A_{11},\, K_{S11}}{\rightleftharpoons}} \text{ERK}\cdot\text{MKK} \quad (11)$$

---------- (Eq. 1)

The following 8 species are restricted to the cytoplasm: MKKK, E1, MKKK·E1, MKKK*, E2, MKKK*·E2, MKK·MKKK*and MKK-P·MKKK* and reactions 1, 2, 3 and 5 can occur only in the cytoplasm. The remaining 15 species and 6 biochemical reactions can occur in both the cytoplasm and the nucleus. Hence we have a total of 38 variables. We assumed identical rate constants for nuclear and cytoplasmic reactions.

In the presence of negative feedback, the input to the cascade is assumed to depend on the level of ERK-PP in the cytoplasm as, $E1_{tot}^{*} = E1_{tot}/(1 + [ERK\text{-}PP]^c/K_I)$. Here $E1_{tot}$ is the constant externally imposed input to the model, $E1_{tot}^{*}$ is the apparent input at any given instant of time, and K_I is the feedback inhibition constant in micromolar. This expression is identical to the one used by Kholodenko (Kholodenko, 2000) in his negative feedback model for MAPK oscillations. In the absence of negative feedback we set $E1_{tot}^{*} = E1_{tot}$.

The following 7 total species abundances need to be conserved during the simulation: $E1_{tot}^{*}$, $E2_{tot}$, $MKKK_{tot}$, MKK_{tot}, ERK_{tot}, $P1_{tot}$ and $P2_{tot}$. While we have a total of 38 variables ($8 + 2\times15$), the mass conservation rules ensure that we only have 31 independent variables for which ODEs describing the fluxes need to be specified. The input to the cascade is the parameter $E1_{tot}$, and this along with 42 other biochemical parameters (35 reaction rate parameters, K_I, and 6 total species concentrations) determines the model dynamics. Given these parameter values, the biochemical reaction fluxes for the 31 variables can be computed. We assume standard mass action kinetics for all reactions except the enzyme-substrate binding steps in reactions 7, 9 and 11. For example, the biochemical reaction flux for MKKK·E1 in the cytoplasm can be written as $b_{MKKK.E1}^{c} = a_1[MKKK]\,[E1] - (d_1 + k_1)\,[MKKK\cdot E1]$ where terms in square brackets refer to species concentrations in micromolar. Expressions can be similarly constructed for the other biochemical fluxes involving mass action kinetics and are listed in (Qiao *et al*, 2007). Enzyme-substrate binding and dissociation in reaction 7 (and reactions 9 and 11) is modeled using a flux term of type $A_7[MKK\text{-}PP][ERK]/\{K_{S7} + [ERK]\} - d_7[ERK\cdot MKK\text{-}PP]$. i.e. the complex formation steps in reactions 7, 9 and 11 are assumed to saturate out as the substrate concentration is increased and in effect become first order reactions that depend solely on the MKK-PP (reactions 7 and 9) or MKK (reaction 11) concentration. The base values for the biochemical parameters that enabled us to match our experimental observations are listed in Table S1.

In addition to the biochemical reaction fluxes, we need to compute transport fluxes for species that are allowed to exist in the nucleus. These transport fluxes are computed by specifying nuclear import and export rate constants for the individual species as per Fujioka et al. (Fujioka *et al*, 2006). In adapting Fujioka et al.'s reactions rates to our model, we had to make a modification to ensure compatibility with our biochemical network. Fujioka et al. constructed a mathematical model for the ERK activation pathway and parameterized it using measurements of the nuclear-cytoplasmic distributions of MEK (MKK in our model) and ERK species. They report distinct transport rate constants for MEK, phosphorylated MEK, ERK, phosphorylated ERK, and MEK-ERK complexes. In their model, MEK has a strong cytoplasmic bias; ERK shows an almost uniform distribution between the nucleus and the cytoplasm and MEK-ERK complexes have an intermediate behavior. Thus, MEK is primarily responsible for dictating the nuclear-cytoplasmic distribution of the various species. Since ERK rather than phosphorylated ERK forms complexes with MEK this ensures that ERK phosphorylation induces an increase in nuclear ERK levels. In contrast to Fujioka et al.'s model, our model involves two ERK phosphorylation steps, and hence we have an ERK-P·MEK complex that is not present in their model. We therefore had to slightly increase the nuclear propensity of phosphorylated ERK

species to ensure ERK nuclear localization comparable to Fujioka's model. Further, we assumed that phosphatases (not modeled by Fujioka et al.) are uniformly distributed between the nucleus and the cytoplasm. The nuclear import (t_i^{imp}) and export (t_i^{exp}) rates for the various species are listed in Table S2.

We combined the biochemical and transport models to derive the concentration fluxes for each of the 15 distinct molecular species that are allowed to exist in both the cytoplasm and the nucleus. The nuclear and cytoplasmic fluxes for any given species *i* can be written as follows:

$$\frac{d}{dt}\begin{bmatrix} x_i^c \\ x_i^n \end{bmatrix} = \begin{bmatrix} b_i^c \\ b_i^n \end{bmatrix} + \begin{bmatrix} -t_i^{imp} & t_i^{\exp}/V \\ t_i^{imp} V & -t_i^{\exp} \end{bmatrix} \begin{bmatrix} x_i^c \\ x_i^n \end{bmatrix} \qquad \text{(Eq. 2)}$$

In the above equation, x_i^c and x_i^n are the cytoplasmic and nuclear concentrations of species; b_i^c and b_i^n are the cytoplasmic and nuclear biochemical fluxes for this species; t_i^{imp} and t_i^{exp} are the nuclear import and export rate constants for this species (Table S2); V is the ratio of cytoplasmic to nuclear volume. We assumed a V value of 6 in our analysis. For the 8 cytoplasmic species, the species fluxes are simply equal to their biochemical flux terms.

ODEs were constructed for the 31 independent variables in our model as described above. We used the inactive state of the system with $E1_{tot}$=0 as the initial condition and solved the ODE system under this condition to obtain the initial species concentrations in the cytoplasm and the nucleus. The only species present at t=0 are E2, P1, P2, MKKK, MKK, ERK and ERK·MKK. For E2 and MKKK the initial concentrations are given by $E2_{tot}$ and $MKKK_{tot}$ respectively, since these species only occur in the cytoplasm. For MKK, ERK and ERK·MKK we solved the governing equation for reaction 11 in Eq. 1 along with the appropriate transport equations from Eq. 2 and the mass balance for ERK and MKK to determine the steady-state cytoplasmic and nuclear concentrations. For P1, which is uniformly distributed between the nucleus and the cytoplasm, the cytoplasmic concentration is $P1_{tot}/2$ and the nuclear concentration is $V \times P1_{tot}/2$. We have similar initial conditions for P2 in terms of $P2_{tot}$. For a given value of $E1_{tot}$ and a given set of biochemical parameters, we computed the initial conditions for the variables as above and then solved the 31 independent ODEs using the MATLAB ode solver *ode15s* to obtain the species concentrations as a function of time.

In order to identify oscillatory parameter sets other than the base set, we fixed the transport rates, and the values of MKK_{tot} and ERK_{tot} at the base values. We generated random values for the other biochemical parameters listed in Table S1 in a range from 1/10th to 10-times the base value. We sampled $MKKK_{tot}$ from 1/3rd to 3-times its base value due to the observed uncertainty in previous estimates for this parameter. As done by Qiao et al. (Qiao *et al*, 2007), we performed this sampling in $\log_{10}$ space. A random value for parameter *i* was thus obtained as $p_i = p_{ic}\,(F^{2r_i - 1})$ where p_{ic} is the base value for parameter *i* (column 1 of Table S1) r_i is a random number between 0 and 1 and F is the maximum allowed fold change for the parameter (F=3 for $MKKK_{tot}$, F=10 for all parameters that were varied). We generated 10,000 random parameter sets. For each parameter set, we used the bifurcation analysis software AUTO to determine the existence of oscillations. We performed this analysis both in the presence and absence of feedback. In the latter scenario the model contains 1 less parameter since K_I does not need to be considered. Single parameter continuation was performed with the input strength $E1_{tot}$ being varied from 0μM to 10 μM to scan for the existence of Hopf bifurcations that would result in oscillations. For

each oscillatory parameter set, the ODE system was solved at the beginning, midpoint and end of the oscillatory regime to determine how much the time period varied within the oscillatory regime. If the time period variation and the width of the oscillatory regime were deemed to be acceptable, we performed a more detailed scan of the oscillatory regime to determine how the time period, rise time and decay time changed as a function of the input strength. The parameter values for the four other oscillatory parameter sets that were discovered to be consistent with the experimental data are presented in Table S1. All of these parameter sets contain the negative feedback loop.

In order to simulate the effect of cell-to-cell parameter variability, we sampled the inputs and biochemical parameters for each theoretical "cell" from log-normal distributions with the mean input given by $E1_{tot}$ and the mean parameters given by the base parameter set respectively. This sampling was done as follows: Let X be the random variable to be randomly sampled and let $Z = \log(X)$ be normally distributed. If X has mean μ_X and coefficient of variation CV_X, then random values for X can be obtained using the MATLAB log-normal random number generator *lognrnd* which requires the following parameters: $\mu_Z = \log(\mu_X) - \log(CV_X^2 + 1)/2$ and $\sigma_Z = [\log(CV_X^2 + 1)]^{0.5}$. Here μ_Z and σ_Z are the mean and standard deviation for the normally distributed variable Z respectively. We set $CV_X = 0.2$ for all parameters of interest and generated random samples as described above. Given the random input and parameter set for a theoretical cell, we used AUTO to determine whether it would oscillate. If it did, then we solved the ODE system to determine the time period, rise time and decay time of the oscillations in the total nuclear ERK concentration.

References

Fujioka A, Terai K, Itoh RE, Aoki K, Nakamura T, Kuroda S, Nishida E, Matsuda M (2006) Dynamics of the Ras/ERK MAPK cascade as monitored by fluorescent probes. *J Biol Chem* **281:** 8917-8926

Huang CY, Ferrell JE, Jr. (1996) Ultrasensitivity in the mitogen-activated protein kinase cascade. *Proc Natl Acad Sci U S A* **93:** 10078-10083

Kholodenko BN (2000) Negative feedback and ultrasensitivity can bring about oscillations in the mitogen-activated protein kinase cascades. *Eur J Biochem* **267:** 1583-1588

Qiao L, Nachbar RB, Kevrekidis IG, Shvartsman SY (2007) Bistability and oscillations in the Huang-Ferrell model of MAPK signaling. *PLoS Comput Biol* **3:** 1819-1826

SUPPLEMENTARY TABLES

Table S1: Biochemical parameters – Base parameter set and other oscillatory parameter sets that match the experimental results

Par No	Par Name	Units	P_0	P_1	P_2	P_3	P_4
1	$MKKK_{tot}$	µM	0.1	6.360E-02	6.200E-02	1.702E-01	2.636E-01
2	MKK_{tot}	µM	1.2	1.200E+00	1.200E+00	1.200E+00	1.200E+00
3	ERK_{tot}	µM	4.8	4.800E+00	4.800E+00	4.800E+00	4.800E+00
4	$E2_{tot}$	µM	0.012	8.350E-02	3.400E-03	9.500E-03	1.500E-02
5	$P1_{tot}$	µM	0.06	1.046E-01	1.210E-01	8.830E-02	1.340E-02
6	$P2_{tot}$	µM	0.05	3.620E-02	4.460E-02	2.022E-01	6.980E-02
7	a_1	/µM/min	1500	1.448E+04	3.349E+03	2.714E+03	1.556E+03
8	a_2	/µM/min	1500	1.501E+02	1.564E+03	2.114E+03	6.574E+02
9	a_3	/µM/min	1500	1.858E+03	5.292E+03	5.080E+03	1.718E+03
10	a_4	/µM/min	1500	6.783E+02	1.400E+03	1.493E+03	1.313E+04
11	a_5	/µM/min	1500	8.442E+03	2.433E+03	1.904E+03	2.658E+02
12	a_6	/µM/min	1500	3.138E+03	3.713E+03	9.549E+03	2.561E+03
13	A_7	/min	15	1.300E+02	2.608E+01	2.469E+01	4.522E+00
14	a_8	/µM/min	1500	5.324E+03	2.996E+03	3.635E+03	8.502E+03
15	A_9	/min	15	8.809E+01	4.726E+01	7.405E+00	1.037E+02
16	a_{10}	/µM/min	1500	3.469E+02	1.465E+04	7.451E+03	4.247E+02
17	A_{11}	/min	15	9.656E+00	5.647E+01	1.203E+02	1.265E+01
18	d_1	/min	4.5	1.482E+00	1.393E+01	9.301E+00	2.107E+01
19	d_2	/min	1.5	9.467E+00	5.083E-01	4.549E+00	4.588E-01
20	d_3	/min	12	3.920E+01	1.797E+00	3.387E+00	2.871E+01
21	d_4	/min	12	1.134E+02	1.454E+01	8.090E+01	4.350E+01
22	d_5	/min	12	5.298E+01	3.260E+01	1.315E+01	6.125E+00
23	d_6	/min	12	2.823E+01	1.934E+00	1.655E+01	2.931E+00
24	d_7	/min	12	5.969E+01	2.491E+00	2.918E+01	2.664E+00
25	d_8	/min	12	2.352E+00	2.577E+00	3.662E+00	7.690E+01
26	d_9	/min	12	6.538E+00	2.013E+01	1.674E+01	1.619E+01
27	d_{10}	/min	12	9.535E+00	5.083E+01	8.075E+00	4.043E+00
28	d_{11}	/min	48	2.106E+01	3.019E+01	2.085E+02	4.024E+02
29	k_1	/min	10.5	1.302E+01	6.493E+01	1.034E+02	1.315E+00
30	k_2	/min	10.5	4.771E+00	1.480E+01	1.604E+00	1.285E+01
31	k_3	/min	10.5	2.536E+01	5.539E+01	2.544E+01	2.787E+00
32	k_4	/min	10.5	5.110E+01	1.177E+01	2.033E+01	2.137E+01
33	k_5	/min	10.5	9.524E+01	7.318E+01	2.475E+01	1.336E+01
34	k_6	/min	10.5	6.826E+00	3.977E+00	1.709E+01	7.337E+00
35	k_7	/min	10.5	5.456E+00	1.492E+01	6.867E+00	1.252E+01

36	k_8	/min	10.5	1.314E+01	1.772E+01	1.909E+00	2.057E+01
37	k_9	/min	10.5	1.055E+00	2.483E+01	9.332E+00	8.899E+00
38	k_{10}	/min	10.5	3.465E+01	1.449E+01	1.270E+01	7.143E+01
39	K_{s7}	µM	0.015	4.910E-02	6.800E-03	3.600E-03	2.600E-03
40	K_{s9}	µM	0.015	8.390E-02	3.100E-03	4.190E-02	2.600E-03
41	K_{s11}	µM	0.015	1.600E-03	5.790E-02	4.800E-03	1.183E-01
42	Ki	µM	0.009	5.200E-03	1.000E-03	1.370E-02	3.900E-03
	$E1_{tot}^{min}$	µM	2.50E-03	4.88E-04	7.38E-05	5.58E-05	1.44E-02
	$E1_{tot}^{max}$	µM	2.70E-01	7.41E-02	1.24E-02	1.05E-02	3.16E+00

The last 2 rows in the table specify the Hopf bifurcation points for each parameter set. Oscillations occur for input strengths that lie between the minimum and maximum values. P_0 is the base parameter set presented analyzed in detail in the manuscript. The behavior of the various parameter sets in the absence of negative feedback is as follows:

P_0 In the absence of negative feedback Hill coefficient = 393

P_1 In the absence of negative feedback system oscillates from E1 = 3.5e-5 to 3.9e-5

P_2 In the absence of negative feedback system oscillates from E1 = 5.2e-5 to 6.7e-5

P_3 In the absence of negative feedback Hill coefficient = 4.9

P_4 In the absence of negative feedback Hill coefficient = 16.8

Table S2: Transport rates

Species type	Applicable molecular species	t^{exp} (/s)	t^{imp} (/s)
MKK	MKK	0.61	0.046
Phosphorylated MKK	MKK-P, MKK-PP	0.54	0.040
ERK	ERK	0.018	0.012
Phosphorylated ERK	ERK-P, ERK-PP, ERK-P·P2, ERK-PP·P2	0.009*	0.012
MKK complexes	ERK·MKK-PP, ERK-P·MKK-PP, MKK-P·P1, MKK-PP·P1, ERK·MKK	0.26	0.035
Phosphatases	P1, P2	0.012#	0.012#

Nuclear export (t^{exp}) and import (t^{imp}) rates for the 15 species that are allowed to exist in both the cytoplasm and the nucleus. Numbers are presented in units of /s to enable direct comparison with Table 5 in (Fujioka *et al*, 2006). These rates were converted to units of /min when they were used in our model. We used a cytoplasm to nuclear volume ratio, V=6 to obtain the concentrations of the species in the nucleus.

* This rate was reported to be 0.013/s in (Fujioka *et al*, 2006), but we reduced it to 0.009 to account for the dual ERK phosphorylation mechanism in our model.

We assume a uniform of distribution of these phosphatases between the nucleus and the cytoplasm.

Supplemental Excel File

This is a 3-tab workbook that contains a comprehensive comparison between the models and parameters presented here and 7 previous models from the literature. File name is: Comparison_of_various_ERK_models

Supplemental Movies

Movies must be viewed with QuickTime version 7 or higher containing the Sorenson Video 3 codec. The viewer is available at no cost at htpp://www.apple.com/quicktime/download/mac.html (for Mac) htpp://www.apple.com/quicktime/download/win.html (for Windows)

Movie S1 – Cells expressing ERK-GFP prior to addition of EGF. 508-nm emission filter. Total time is 15 minutes, images at 1-minute intervals, magnification 60X.

Movie S2 – Cells expressing ERK-GFP after addition of EGF. 508nm emission filter. Total time is 2 hours, images at 1-minute intervals, magnification 60X. The data from these cells are shown in Figs. 1B and 1C of the main text.

Movie S3 – Same sample as Movie S2, but imaging the red channel (604nm emission filter).

Movie S4 – Cells grown at a density of 1×10^4 cells per cm^2 stimulated at 5 minutes with 1 ng/ml EGF. Total time is 2 hours, images at 1-minute intervals, magnification 20X. Data from these cells are shown in Figs. 2B and 2C of the main text.